Parallel measurements and engineering simulations of conversion, shear modulus, and internal stress during ambient curing of a two-component epoxy coating

Qiong Li, Claus Erik Weinell, Søren Kiil [ORCID]

Abstract Macroscopic crack initiation and propagation, as a result of internal stress, poses a threat to the performance of protective coatings. In demanding environments, such as corner geometries and saltwater exposure, the cracks may accelerate substrate corrosion and potentially lead to collapse of infrastructure. The present work is focused on the underlying mechanisms of curing-induced internal stress and investigates the dynamics of the parallel processes of crosslinking reactions and evolution of mechanical properties for a solvent and pigment-free epoxy resin cured with a diamine hardener. Experimental techniques, applied at room temperature and constant relative humidity, include attenuated total reflection-Fourier transform infrared (ATR-FTIR) spectroscopy, advanced rheometry, dynamic mechanical thermal analysis (DMTA), and a beam deflection device. When taking post-vitrification mobility control into account, the reaction kinetics behind the crosslinking and network development could be simulated with a modified Kamal–Sourour model. In addition, engineering models for simulation of coating modulus, volumetric shrinkage, and internal stress as a function of conversion were proposed and found to be in good agreement with experimental data. This allowed, by comparing the magnitudes of the modulus and the internal stress, for evaluation of whether premature cracks are expected to initiate. Furthermore, we show that the curing-induced internal stress development is strongly influenced by the current coating elastic modulus and film thickness, highlighting the effect of coating property transients. The experimental techniques and engineering modeling tools collected can be used to evaluate, without demanding computational complexities, the simultaneous development of coating modulus and curing-induced internal stress.

Keywords Internal stress, Two-component thermoset epoxy coating, Chemical shrinkage, Modulus evolution, Conversion

Abbreviations

ATR-FTIR	Attenuated total reflection Fourier transform infrared spectroscopy
DMTA	Dynamic mechanical thermal analysis
CHILE	Cure hardening instantaneously linear elastic
PVE	Pseudo-viscoelastic
BMI	Bismaleimide
T_g	Glass transition temperature, °C
FEM	Finite element method
BFDGE	Diglycidyl ether of bisphenol F
MXDA	M-xylylenediamine
WFT	Wet film thickness, μm

Supplementary Information The online version contains supplementary material available at https://doi.org/10.1007/s11998-022-00652-8.

Q. Li, C. E. Weinell, S. Kiil (✉)
The Hempel Foundation Coatings Science and Technology Center (CoaST), Department of Chemical and Biochemical Engineering, Technical University of Denmark, (DTU), Building 229, 2800 Kgs. Lyngby, Denmark
e-mail: sk@kt.dtu.dk

List of symbols

X_E	Conversion of epoxide groups in epoxy
$A_{915,t}$	Absorbance area of epoxide groups at different measurement times

$A_{1250,t}$	Absorbance area of reference peak at different measurement times
$A_{915,0}$	Absorbance area of epoxide groups at initial time
$A_{1250,0}$	Absorbance peak area of reference peak at initial time
LVR	Linear viscoelastic response
h	Coating thickness at different measurement times, μm
h_0	Initial coating thickness at the beginning of the measurement, μm
E_s	Substrate Young's modulus, MPa
t_s	Substrate thickness, mm
d	Deflection at different measurement times, mm
t_c	Coating thickness, mm
L	Coating length, mm
E_c	Coating Young's modulus, MPa
$[E]$	Epoxide group concentration
k_1	Reaction rate constant of autocatalytic primary amine reaction resulting from OH groups generated during reaction, h^{-1}
$[A_1]$	Primary amine concentrations
$[EOH]$	Variable concentration of hydroxyl groups formed during curing that can catalyze the reactions
k_{1c}	Reaction rate constant of impurity-catalyzed primary amine reaction resulting from OH groups in initial formulation, h^{-1}
$[ROH]$	Constant concentration of impurities exists in coatings that can catalyze the reactions
k_2	Reaction rate constant of autocatalytic secondary amine reaction resulting from OH groups generated during reaction, h^{-1}
$[A_2]$	Secondary amine concentrations
k_{2c}	Reaction rate constant of impurity-catalyzed secondary amine reaction resulting from OH groups in initial formulation, h^{-1}
t	Curing time, h
$k_{1,nc}$	Reaction rate constant of noncatalytic reaction between epoxy and amine in initial formulation, h^{-1}
$k_{2,ac}$	Reaction rate constant of autocatalytic reaction resulting from OH groups in initial formulation and OH groups generated during reaction, h^{-1}
$X_{E,vit}$	Degree of conversion at vitrification
D_c	Parameter to relate α_{gel} and the vitrification effect
$X(t)$	Conversion as a function of time
$G'(t)$	Storage shear modulus as a function of time, Pa
G'_0	Initial modulus before curing, Pa
G'_∞	Final modulus after curing, Pa
X_∞	Final conversion after 120 h isothermal curing
G'	Storage shear modulus, Pa
K	Bulk modulus, Pa
$K(X)$	Bulk modulus as a function of conversion, MPa
$G'(X)$	Storage shear modulus as a function of conversion, MPa
I	Identity tensor
E	Young's modulus, MPa
G	Storage shear modulus, MPa

Greek

|	
ε_V	Volumetric shrinkage
v_c	Coating Poisson's ratio
v_s	Substrate Poisson's ratio
$\varepsilon_{cure}(t)$	Curing-induced volumetric shrinkage as a function of time
v	Poisson's ratio
σ	Internal stress, MPa
$\sigma(t)$	Internal stress as a function of time, MPa

Introduction

Due to their chemical resistance and mechanical and thermal stabilities, two-component epoxy coatings are widely used industrially to protect steel constructions, such as ships and wind turbine towers, against corrosion.[1–4] However, defects in anticorrosive coatings, such as microcracks and voids, originating from the application, curing, or inappropriate formulation, are a potential threat to the performance. In or around the defects, barrier properties can be compromised, leading to excessive ingress of saltwater. This, in turn, initiates localized corrosion of the underlying structure, in the form of pitting or crevice corrosion, which can, if not handled, induce catastrophic disasters, such as pipeline explosions or bridge collapses.[3,5,6]

The origin of cracks and other defects in anticorrosive coatings can often be attributed to the development of internal stress, which either forms during the curing process and/or develops when external factors, such as temperature, humidity, water absorption, or mechanical stress, vary.[7] Generally, differences in the thermal or hygroscopic expansion coefficients of the substrate and coating layers induce compressive or tensile stresses, which drive the crack initiation and propagation with changes in exposure conditions.

When a thermoset epoxy coating cures, the liquid film gradually solidifies a process driven by crosslinking

reaction(s) and/or solvent evaporation. The coating builds molecular weight, glass transition temperature, and mechanical properties, while the volume shrinks. Prior to the gelation point, the viscosity increases, but the viscous stress remains insignificant. At the so-called vitrification point (which may be coating depth-dependent[8]), the glass transition temperature of the coating network (including any solvent present) becomes equal to the curing temperature, and, due to a strong adhesion at the coating–substrate interface, the volumetric shrinkage gets constrained, which leads to a tensile in-plane stress development.[9] In some cases, as illustrated in Fig. 1a, the internal stress exceeds the strength of the coating and can initiate cracks.[9] Subsequently, when the driving energy for cracking, which is influenced by the local stress and the film thickness, exceeds the critical fracture energy (defined as the amount of energy that must be concentrated on the crack tip before a crack propagates), brittle crack propagation will occur and the energy required to make the crack propagate per unit area is regarded as the fracture toughness.[10–13] An example of the morphology of a crack is provided in Fig. 1b, where cracks, resulting from curing-induced internal stress within a novolac epoxy/cycloaliphatic amine coating, were observed with optical microscopy.

Curing-induced internal stress can also concentrate around pigments and fillers. The particulates represent discontinuities in the matrix, and the states of stresses are different around these, resulting in more localized
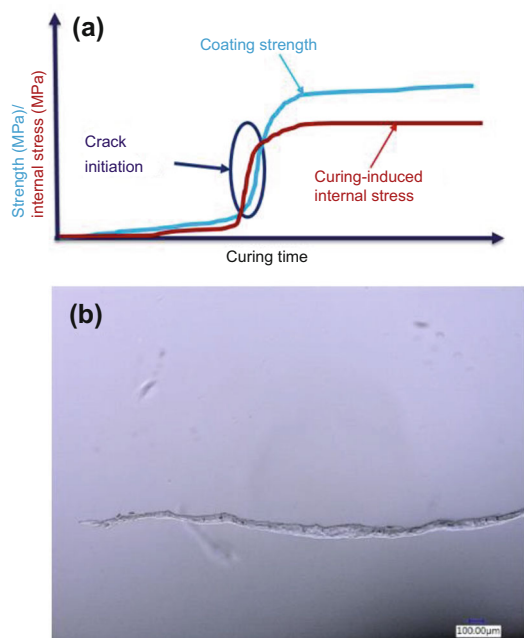
Fig. 1: (a) Schematic illustration of the coating strength and the internal stress development during curing. (b) Optical micrograph (top view) of a crack in a pigment-free novolac epoxy/cycloaliphatic amine coating with a dry film thickness of 105 μm after 24 h of curing at 23°C. The scale is shown in the micrograph

defects.[9] Generally, coatings exhibit a critical cracking thickness, which depends on the formulation and exposure conditions and can range from about 50 nm–500 μm.[14]

To control and reduce stress-related defects and cracks in coatings, it is essential to investigate the curing-induced internal stress development. For quantification in polymeric coatings, the following nondestructive techniques, reviewed in references (9, 15–17), have been employed: photoelasticity,[18] time-resolved fluorescence,[19] Raman spectroscopy,[20] X-ray and neutron diffraction with crystalline particle embedding,[21] and beam deflection.[9,22–25] The latter technique is rather easy to implement, and the sample deflection development can be recorded with various techniques, such as microscopy, capacitance gauges, and laser-based distance/position sensors.[9]

Earlier works investigated the effects on internal stress of the binder/hardener formulation, temperature, humidity, fillers, pigmentation, and solvent content.[9,26–30] However, in these studies, the coatings elastic moduli and thicknesses were assumed constant during curing, which leads to inaccurate assessment of the curing-induced internal stress. In addition, when evaluating the internal stress using the deflection method, a constant coatings thickness assumption will, according to Francis et al.[9], result in underestimation of the internal stress values.

Although many articles have focused on epoxy coating mechanical properties, most of the earlier works measured the elastic modulus on fully cured samples with DMTA, 3-point bending test, or the tensile testing method.[31–34] Such an approach does not capture the influence of curing reactions on the coating property evolution. Alternatively, advanced rheometers and other instruments have been used to monitor the elastic modulus evolution. However, parallel plate rheometry with an oscillatory shear measurement works well for coatings at low degrees of curing (i.e., prior to gelation). Post-gelation, other rheometry techniques, such as 3-point bending or tensile testing, should be used to estimate the coating modulus.[31]

To investigate the curing-dependent mechanical properties and/or shrinkage evolution in epoxy coatings, mathematical modeling has been used. Zobeiry et al.[35] investigated the so-called Cure Hardening Instantaneously Linear Elastic (CHILE) model, a pseudo-viscoelastic (PVE) and a complex viscoelastic (VE) model in their ability to estimate the dynamics of the mechanical properties evolution. They specifically investigated two commercial epoxy resins over a temperature ramp, hold-on, and cooling-down curing ramp. It was found that the complex VE model can be simplified to the PVE model by introducing time-dependent elastic modulus with good agreement in the simulated internal stress. Using a constant elastic modulus, the complex VE model can be further simplified to the CHILE model. However, this simplification can bring imprecision because the time-dependent mechanical property evolution of the cured

sample was ignored. Radue et al.[36] tried to expand the molecular simulations to epoxy–amine curing with multiple reactions. They studied the thermomechanical property evolution in a Matrimid-5292 bismaleimide (BMI) resin, with five curing reactions. Their results show that as conversions increase, both glass transition temperature and Young's modulus increase and the simulated Young's modulus agreed well with the experimental results. Simon et al.,[37] for isothermal curing and post-gelation, built a model to estimate viscoelastic properties of a commercial epoxy. They found that the storage modulus begins to build at the gelation point and increase with higher values of conversion. At the vitrification point, the storage modulus exhibited a sharp increase. Rabearison et al.[38] proposed a finite element method (FEM) coupling model to predict the localized conversion, elastic modulus, shrinkage, and internal stress within an epoxy matrix, with an approach to predict localized stress magnitudes. Their model needs calibration against experimental data.

Using diffusion-controlled reaction kinetics, coupled with a temperature- and conversion-dependent viscoelastic relaxation model, Alig et al. simulated the curing-induced internal stress in epoxy coatings with a generalized Hookean model. They compared simulations to coating properties, measured by temperature-modulated calorimetry, DMTA, ultrasonic spectroscopy, light scattering, and laser scanning dilatometer.[39–41] The advantage of this approach was the possibility to simulate nonisothermal curing and realistic curing programs. For test of material equations and parameter sets, the evolution of stress, by an iterative numerical approach for a radial symmetric model geometry (and later extended to coating layers), was conducted. In a second step, the models were implemented into a FEM code (ABAQUS). For the evolution of conversion, shrinkage, shear storage modulus, Poisson's ratio, glass transition temperature, and internal stress in coatings, the experimental results were found to be in good agreement with simulations. The model was partially adapted for simulation in the electronics industry (i.e., encapsulations) and further modified and adapted to UV-curing of coatings.[42] More recently, it was also used for simulation of humidity and temperature-induced stress in coatings during weathering. However, although this model provides high-precision calculations for curing-induced internal stress and advanced corporations may go to this level, the evaluation of time-dependent parameters and computational complexities involved render it perhaps less useful for routine industrial applications.

With the aim of providing industrial guidelines for reduction of internal stress-related crack formation in thermoset epoxy coatings, the present work quantifies the dynamics between crosslinking reactions, mechanical properties, and internal stress. This, in turn, can support the development of anticorrosive coatings with superior barrier properties and long durability. The strategy of the investigation is to quantify, in parallel, the curing-induced internal stress, the curing kinetics, the volumetric shrinkage, and the mechanical property evolution. For the analyses, IR spectroscopy, 3D profilometry, advanced rheology, and dynamic mechanical analysis (DMTA) are used. In addition, to evaluate the development of internal stress as a function of conversion, volumetric shrinkage, and the coatings storage shear modulus, an overall engineering model, based on easy-to-handle equations from previous investigations, is collected. Finally, simulations and experimental data for the internal stress are compared and discussed.

Experimental

Materials and coating preparation

An anticorrosive EPON 862/MXDA coating with an amine/epoxy functional group stoichiometric ratio of 1.0 was formulated. The binder was a solvent-free diglycidyl ether of bisphenol F (BFDGE) epoxy resin manufactured by Hexion B.V. with an epoxy equivalent weight of 169 g/mol, and used as received. A solvent-free m-xylylenediamine (MXDA) supplied by Sigma-Aldrich was used to prepare MXDA-BFDGE adduction, and the 7.5% adducted MXDA-BFDGE was used as a hardener. Molecular structures of EPON 862 and MXDA are shown in Fig. 2.

Application of the pigment and filler-free EPON 862/MXDA coatings were initiated by mixing the binder and hardener. For the degree of conversion measurements, the wet film thickness (WFT) was controlled using an Elcometer 3580 casting knife film applicator, which could adjust film thickness from 0 to 6 mm with increments of 10 μm to 300 ± 10 μm. This is a typical heavy-duty epoxy-based coating thickness.
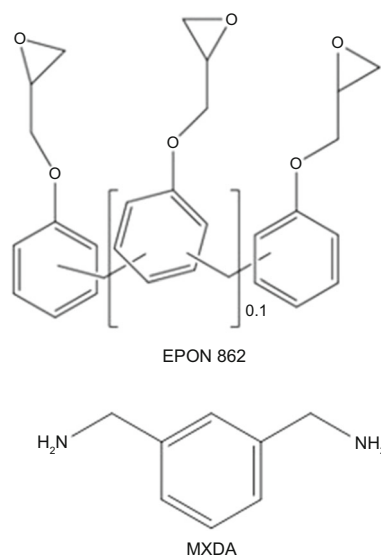

Fig. 2: Molecular structures of epoxy EPON 862 and MXDA

The coatings were applied on a 0.1-mm-thick plastic substrate (supplied by Erhvervsskolernes Forlag, Denmark), and the samples stored in an Aralab climate chamber for 120 h with the temperature and relative humidity set to 23 ± 0.5°C and 35 ± 1%, respectively.

FTIR spectroscopy

The reactant (epoxy) conversion as a function of curing time was monitored with a Thermo Scientific Nicolet is50 ATR-FTIR spectrometer and calculated from equation (1)

$$X_\mathrm{E} = 1 - \frac{A_{915,t}/A_{1250,t}}{A_{915,0}/A_{1250,0}} \qquad (1)$$

where X_E is the conversion of epoxy (epoxide) groups. The absorbance peak at 915 cm^{-1} was assigned to epoxide, and the one at 1250 cm^{-1} to the phenylene group (used as a reference peak, see Fig. 3). For the evaluation of the repeatability, three samples were used for each measurement.

Dynamic mechanical thermal analysis (DMTA) measurements

An advanced rheometer DHR-2 (TA Instruments) was used to monitor the shear storage modulus evolution through curing. For strain-controlled oscillation mode, an excessive liquid coating sample was placed between two 25-mm-diameter parallel plates to make sure that the gap between the parallel plates is filled up. For the removal of the overflow, tissue was used. The measurement was taken with a fixed gap of 200 μm, a frequency of 1 Hz, and a shear strain of 6.25%. The gelation point was taken as the point in time where the storage modulus became equal to the loss modulus, and vitrification time was chosen as the time of maximum storage modulus. ATR-FTIR was used to measure the conversion at the gelation and the vitrification points. For DMTA tension test, free films (20 × 10 × 0.3 mm^3) at different curing times were prepared by pouring the liquid epoxy/amine mixture into silicone molds and letting the samples cure in a climate chamber. The oscillation-temperature ramp procedure was from 30 to 150°C with a heating rate of 1°C/min and a frequency of 1 Hz.

Tensile test

Tensile test samples were prepared with the same method as the DMTA free-film samples, and testing was performed using an advanced rheometer DHR-2 (TA Instruments). To track the strength of the curing coating at different values of time, the tensile procedure was conducted at 23°C with a linear tension rate of 5 μm/s.

Curing shrinkage measurement

The curing shrinkage measurements were taken using an optical 3D profilometer (KEYENCE VR-3000). Silicone molds, as shown in Fig. 4a, were used to prepare samples with a controlled thickness of 300 μm. The sample thickness was monitored with a profilometer at different curing times (Fig. 4b), and the area for analysis, using silicone molds and profilometer software, was kept constant and controlled throughout the curing. To obtain the sample thickness information, the left edge of the sample (light blue line in Fig. 4c) was used as reference and the thickness profile results of the yellow line (shown in Fig. 4d), red line, and the blue line were used to achieve the average thickness profile. Any deformation of the silicon molds and sticking of the epoxy resin to the walls of the molds, due to epoxy vitrification, were considered insignificant
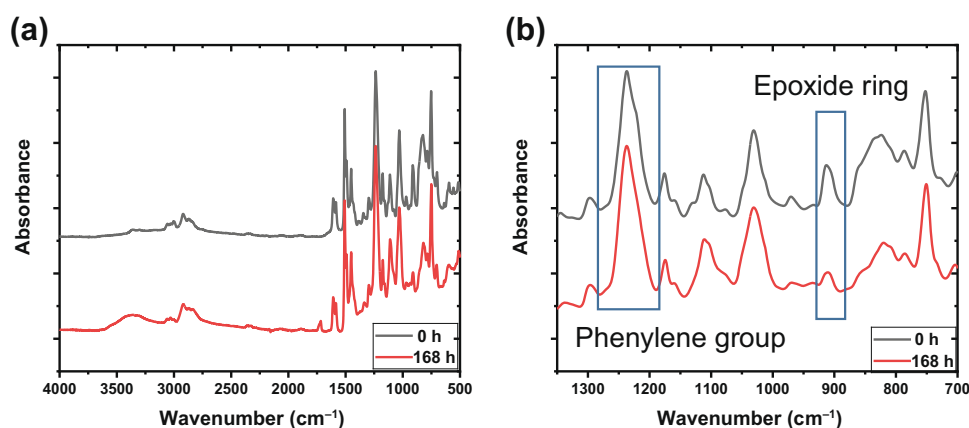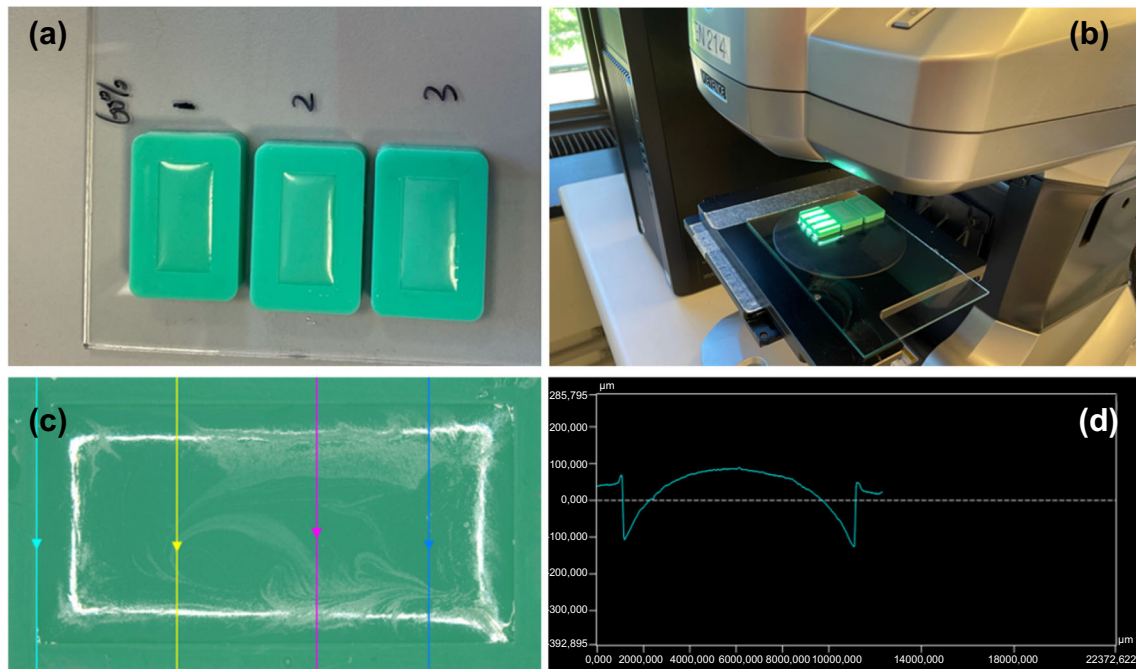

Fig. 3: (a) The full FTIR spectrum of epoxy EPON 862/MXDA system before (0 h) and after curing (168 h). (b) Close-up of the relevant wavelengths with indication of the epoxide ring and phenylene group peaks used in the calculation of the reactant conversion

Fig. 4: Schematic diagram of coating thickness monitoring with a 3D profilometer. (a) Samples prepared in silicone molds to monitor coating thickness, (b) coating thickness measurement (in the silicone mold) using a 3D profilometer, (c) locations used to analyze the thickness profile, and (d) thickness profile of the yellow line in (c) (Color figure online)

and, consequently, ignored.[43] To determine the current coating thickness, five points were selected along each of the three lines.

The current film thickness was used to calculate the reaction-induced volumetric shrinkage using the following equation

$$\varepsilon_V = \left(1 + \frac{1}{3}\left(\frac{h - h_0}{h_0}\right)\right)^3 - 1 \tag{2}$$

where ε_V is the volumetric shrinkage, h the current and h_0 the initial coating thickness.[44] Note that upon shrinkage, ε_V attains negative values.

Internal stress measurements

To monitor the curing-induced internal stress, the coatings were applied on 0.1-mm-thick 316L stainless steel shims with a length of 200 mm and a width of 15 mm (Fig. 5a). Prior to application, the substrates were cleaned with ethanol. Using an Elcometer 3580 applicator, the wet coating thickness was controlled to $300 \pm 10 \ \mu m$. The coated samples were placed horizontally in a climate chamber under a relative humidity of $35 \pm 1\%$ and a temperature of $23 \pm 0.5°C$ for 4 h. To omit the influence of gravity and make use of position detective sensors (Fig. 5b), samples were fixed vertically with a clamp, allowing deflection at the free end.
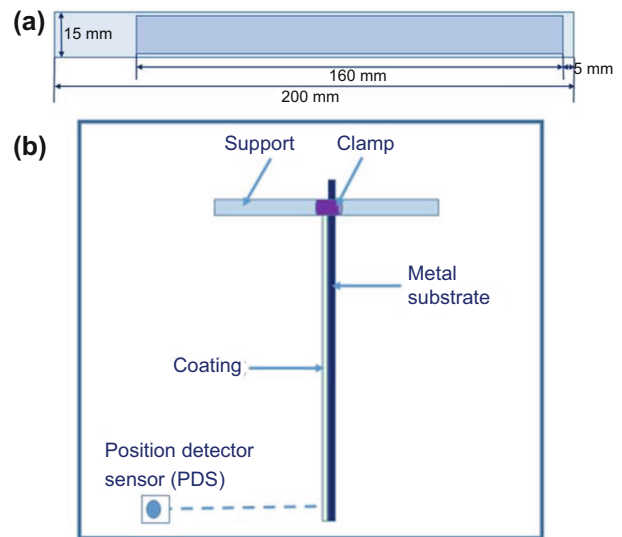
Fig. 5: The beam deflection device for monitoring of curing-induced internal stress. (a) Schematic illustration of a coated metal deflection sample (top view). (b) Setup for beam deflection method to monitor the curing-induced internal stress, mounted vertically at the top end

Using the deflection data recorded, the internal stress for a coating is calculated from the following equation[9]

$$\sigma = \frac{E_s t_s^3 d}{3 t_c L^2 (1 - v_s)(t_c + t_s)} + \frac{E_c d (t_s + t_c)}{L^2 (1 - v_c)} \tag{3}$$

Here σ is the internal stress, E_S the substrate Young's modulus, t_s the substrate thickness, d the measured deflection, t_c the coating thickness, L the coating length, v_s the substrate Poisson's ratio, E_c the coating Young's modulus, and v_c the Poisson's ratio of the coating. The assumptions underlying equation (3) are[9]:

- Curing-induced internal stress is biaxial within the coating.
- Adhesion between the coating and the substrate is strong.
- The mechanical properties of the substrate and the coating are isotropic.

Mathematical modeling

A dynamic engineering model to describe curing-induced internal stress in solvent-free coatings at room temperature is now described. The model takes into account the conversion of epoxy groups, the development in coating modulus and shrinkage, and the development of curing-induced internal stress. The assumptions underlying the model are:

- The coating is isothermal (ambient temperature) with no compositional or mechanical property gradients.
- Prior to gelation, curing shrinkage can be neglected.
- The Poisson's ratio of the coatings is at all times 0.3. This value has been widely used in epoxy coating mechanical property modeling.[45]
- No crack formation in the coated samples during curing.
- The etherification reaction is insignificant and can be ignored at ambient curing conditions.
- The reaction rates of primary and secondary amine are the same.
- Both the noncatalytic reaction between epoxy and amine and the reactions catalyzed by impurities and hydroxyl groups formed during curing are considered.

Curing kinetics

For the curing kinetics of epoxies, equation (4), which was derived based on the reactions listed in reference (46, 47), is used:

$$-\frac{\mathrm{d}[E]}{\mathrm{d}t} = k_1[E][A_1][\mathrm{EOH}] + k_{1c}[E][A_1][\mathrm{ROH}] \\ + k_2[E][A_2][\mathrm{EOH}] + k_{2c}[E][A_2][\mathrm{ROH}] \quad (4)$$

where $[E]$ is the concentration of epoxide groups. k_1 and k_2 denote the reaction rate constants of the autocatalysis reaction, k_{1c} and k_{2c} represent the reaction rate constants of the impurity-catalyzed reactions, and $[A_1]$ and $[A_2]$ are the concentrations of primary and secondary amines, respectively. The constant impurity concentration in the coatings, [ROH], can catalyze the reaction between epoxy groups and amine groups, and [EOH] is the concentration of hydroxyl groups that can catalyze the reaction formed in the epoxy and amine reactions.

The conversion of epoxy groups (X_E) is equal to one minus the current epoxy group concentration divided by the initial epoxy group concentration, and equation (4) can be rewritten into:

$$\frac{\mathrm{d}X_E}{\mathrm{d}t} = k_{1,nc}(1 - X_E)^2 \left(X_E + \frac{k_{2,ac}}{k_{1,nc}} \right) \quad (5)$$

where $k_{1,nc}$ is the reaction rate constant of the noncatalytic reaction between epoxy and amine in the initial formulation and $k_{2,ac}$ denotes the reaction rate constant of the autocatalytic reactions catalyzed by the OH groups from the initial formulation and the OH groups generated during curing.

Equation (5) is not able to account for coating vitrification effects, and the model assumes complete conversion at any temperature despite the fact that the degree of conversion depends on curing temperature. This may result in an inaccuracy, especially for epoxies cured at room temperature. In order to account for the vitrification effect, the model can be extended to equation (6)[42,46,48–52]:

$$\frac{\mathrm{d}X_E}{\mathrm{d}t} = k_{1,nc}(1 - X_E)^2 (X_E + k_{2,ac}) \left(\frac{1}{1 + \exp\left(D_c(X_E - X_{E,vit})\right)} \right) \quad (6)$$

Here, $X_{E,vit}$ is the degree of conversion at vitrification, and D_c is a constant.

Chemical strain model

Li et al.[53] proposed a model to fit the chemical shrinkage of a commercial epoxy as a function of the degree of conversion with two linear equations before and after the gelation point. However, in the current work, because it is widely accepted that curing-induced internal stress can only be developed after gelation/vitrification point and the shrinkage before gelation has little influence on the internal stress,[9,54] the chemical shrinkage prior to the gelation point was neglected. Thus, the linear equations [equations (11) and (12) shown in Fig. 7c] were used in the current work to model the chemical shrinkage as a function of conversion.

Elastic behavior of coating

To quantify the influence of conversion on the storage shear modulus, the following equation is used[55]:

$$X(t) = \frac{\log(G'(t)) - \log(G'_0)}{\log(G'_\infty) - \log(G'_0)} X_\infty \tag{7}$$

Here, $X(t)$ is the conversion as a function of time, G' the storage shear modulus, G'_0 the initial modulus, G'_∞ the final modulus, and X_∞ the final conversion after 120-h isothermal curing. Note that in this simplified equation, the influence of temperature, induced by the exothermic crosslinking reactions, and the effects of cure-dependent stress relaxation were ignored (for more elaborate calculations, see reference (37, 40, 42, 56).

Using a DFT of 300 μm and a substrate thickness of 0.1 mm, heating effects (an increase of 0.3°C was measured) could safely be ignored in our experiments. In addition, Figure S1 in supplementary information shows that the curing coating was dominated by viscosity prior to gelation (and vitrification, which was coincident). However, after around 5 h of curing, the system was elastically dominated. Consequently, the relaxation effect, which requires complex viscoelastic modeling, was ignored in this work.

Equation (8) can be used to calculate the internal stress with the shear modulus G' from equation (7), and bulk modulus, K, from equations (9) and (10)[57]

$$\sigma(t) = \left[K(X) - \frac{2}{3}G'(X)\right]\mathrm{tr}(\varepsilon_{\mathrm{cure}}(t)) \cdot I + 2G'(X) \\ \cdot \varepsilon_{\mathrm{cure}}(t) \tag{8}$$

Here, $\sigma(t)$ is the internal stress as a function of time and $\varepsilon_{\mathrm{cure}}(t)$ is the curing-induced volumetric shrinkage. I is the identity tensor, and $K(X)$ and $G'(X)$ are bulk modulus and shear modulus as a function of conversion, respectively.

For isotropic materials, the Young's modulus, E, and the bulk modulus, K, can be calculated using equations (9) and (10), where G is the shear storage modulus and v is the Poisson's ratio, assumed constant (value of 0.3) throughout the curing process.

$$E = 2G(1 + v) \tag{9}$$

$$K = \frac{E}{3(1 - 2v)} \tag{10}$$

Results and discussion

The experimental results for conversion, modulus evolution, shrinkage, and curing-induced internal stress of epoxy coatings will now be described, followed by a comparison of model simulations with experimental data.

Evolution of coating properties during curing

The full experimental transients of coating properties during curing are shown in Fig. 6, including conversion,
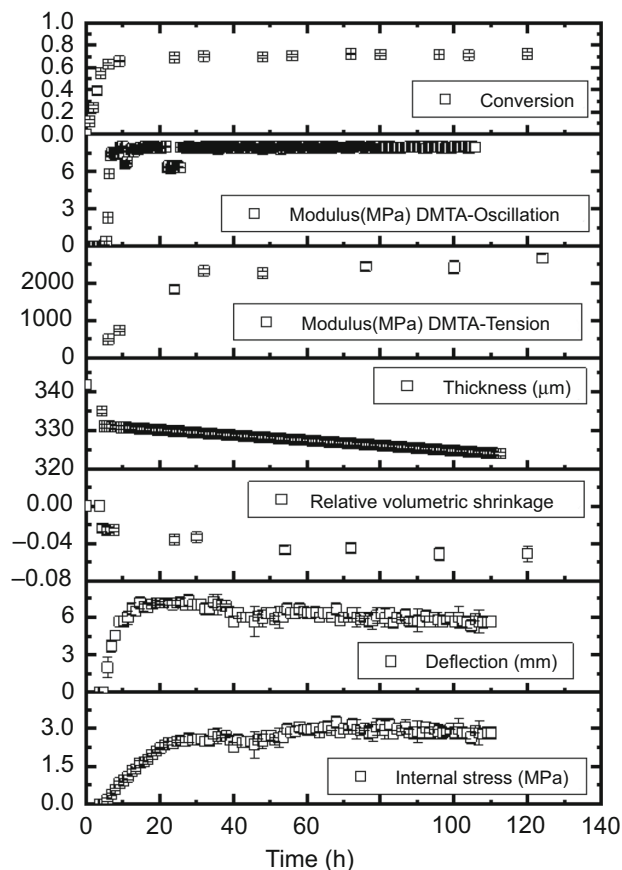
Fig. 6: Experimental data of coating properties evolution during curing at 23±0.5°C for the solvent- and pigment-free EPON 862/MXDA binder system. The coating properties monitored were (from top to bottom): epoxy groups conversion, coatings storage shear modulus measured with DMA oscillation, coatings elastic modulus measured with DMA tension, coating thickness, relative volumetric shrinkage, deflection, and internal stress measured with the deflection method. Standard deviations are provided with error bars for all measurements

elastic modulus, film thickness, volumetric shrinkage, deflection in beam deflection, and internal stress estimated from the beam deflection measurements.

During the first four hours, the conversion (measured with ATR-FTIR) increases fast. After this point, as a result of vitrification, where all reactions become mobility-controlled,[58] the rate of consumption of epoxy groups rapidly decreases and the conversion exhibits a very slow increase. After 24 h, the conversion comes close to a plateau value around 0.72.

For the storage modulus (monitored with DMTA oscillation-time test), an initial slow build in the first 3.2 h is seen, after which the storage modulus, due to gelation, exhibits a steep increase. Unlike the degree of conversion, which reached a plateau after 24 h, the storage modulus, due to gelation/vitrification, reaches a plateau already after four hours because the gap adjustments are no longer possible and the sample cannot fully fill the gap, resulting in a significantly smaller storage shear modulus.[31]

To analyze the influence of conversion on the bulk storage modulus, DMTA tension experiments were conducted and the measured elastic modulus increases with curing time after 6 h and reaches a constant value after around 72 h, indicating that the DMTA tension measurement is better at representing the influence of conversion on modulus evolution than the oscillation-time recordings.

From 0 to 4.5 h (prior to vitrification), the coating thickness decreases fast (18 μm in absolute values), as a result of relatively fast crosslinking reactions. Subsequently, the thickness exhibits a very slow decrease, 8 μm in absolute value, after 120 h.

The coating shrinkage, due to crosslinking, increases fast after the gelation point (3.5 h); the chemical shrinkage is − 0.0237 (relative value) at 4.5 h. Later, the shrinkage shows a downward tendency with a fluctuation within a narrow range and settles on − 0.050 (relative value) after 120 h of curing.

The deflection monitored with laser sensors shows an increase from 4 to 10 h and then slowly reaches the maximum deflection at about 20 h. Later, the deflection exhibits fluctuation and a downward tendency as a result of the coating modulus increase and the film thickness decrease.

A measurable internal stress begins to build after four hours and then increases with curing time to around 20 h, where it reaches a plateau around 2.2 MPa. Later, the internal stress exhibits a slow increase after 40 h and reaches the maximum around 3.0 MPa at 60 h. Afterward, fluctuations, as a result of the simultaneous internal stress development and stress relaxation, are seen.

It should be noted that compared to deflection, a delayed internal stress build-up, as a result of the coating modulus increase and the film thickness decrease, is evident. More importantly, although the deflection exhibits a decrease after 20 h, the internal stress, due to the coating modulus evolution and film thickness change being included in the calculation,

continues to increase. This shows that nonconstant coating modulus and thickness uses are preferable when estimating the internal stress with the deflection method.

Comparison of model simulations with experimental data

The experimental and simulated coating properties evolution during curing is summarized in Fig. 7.
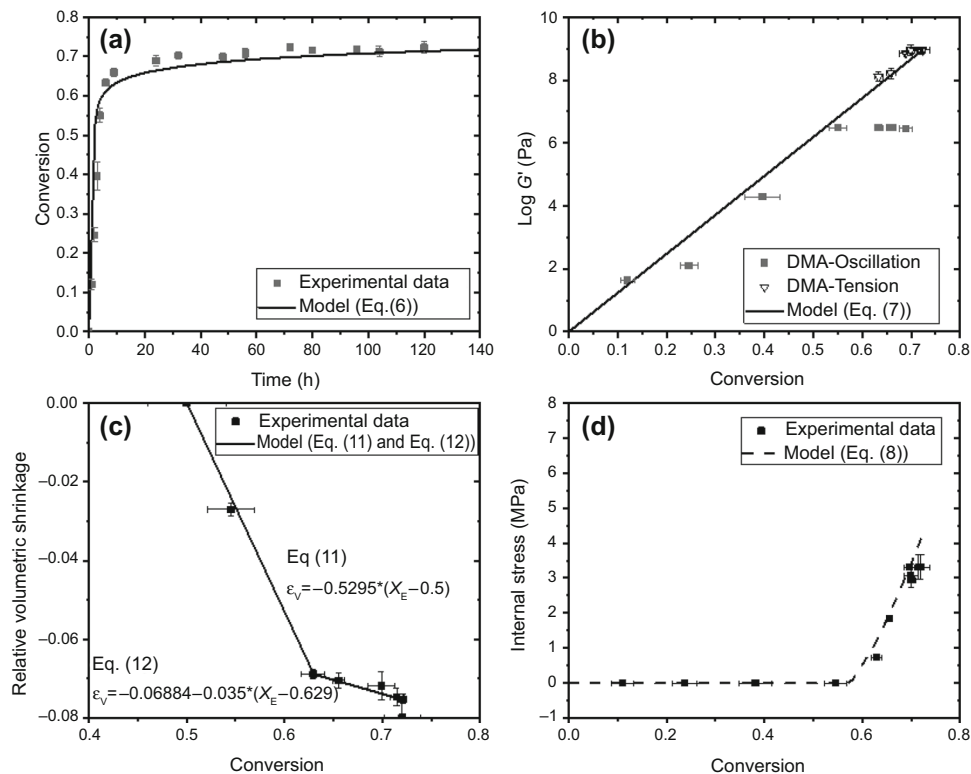
A comparison of experimental conversion–time data with simulations of the modified Kamal–Sourour model (equation 6) is shown, and a good agreement is evident (Fig. 7a). The following parameter values were adjusted: $k_{1,nc}$, $k_{2,ac}$, and D_c, while the parameter $X_{E,gel}$ was estimated experimentally with the DMA oscillation test.

Figure 7b shows a comparison between the simulated modulus as a function of conversion and measured modulus from DMTA experiments correlated with ATR-FTIR results at different curing times. Simulations using equation (7) agree well with the experimental data. The parameter α_∞ was measured with ATR-FTIR, and G'_0 and G'_∞ are experimentally determined with oscillation–time DMTA measurements and tension DMTA measurement, respectively.

Figure 7c shows a comparison between the simulated chemical shrinkage as a function of conversion and the measured shrinkage correlated with conversion. Using equations (11) and (12) with acceptable agreement, the two-step shrinkage evolution before and after the vitrification point can be simulated.[59]

Figure 7d shows a comparison between the simulated internal stress as a function of conversion with equation (8) and the measured internal stress with the deflection method. It can be seen that the experimental data agree well with the modeling result, while after the coating reached high conversion (around 0.7), the modeling results exhibit higher internal stress than the experimental data. This is due to the inherent heterogeneities in deflection samples and internal stress relaxation, which can lead to microscale defects and crack initiations. Such phenomena often seen around heterogeneities result in a slight decrease in the measured deflection and the measured internal stress.

A comparison of the transient coating strength and the curing-induced internal stress in epoxy/MXDA coatings is shown in Fig. 8. It can be seen that the coatings strength is much larger than the internal stress if we assume that there is no stress concentration effects (i.e., a stress concentration factor of 1.0 in the left-hand figure in Fig. 8), indicating that no defects and cracks will be formed. In reality, heterogeneities are inevitable in epoxy coatings[60] and stress can concentrate around these. If we assume a relatively low stress concentration factor of 5.0 (right-hand figure in Fig. 8), meaning that the stress is amplified five times after stress concentration around hetero-

Fig. 7: Comparison of simulations with experimental data of epoxy/MXDA coatings properties evolution. (a) The measured conversion of the epoxy group in the system and the modified Kamal–Sourour model. Adjustable parameters are: $k_{1,nc} = 0.4$ h^{-1}, $k_{2,ac} = 0.43$ h^{-1}, $D_c = 30$, (b) Coating modulus evolution as a function of conversion and the proposed model. Parameters are Log G'_0=0, Log G'_∞=8.958, and $X_\infty = 0.723$, (c) Relative volumetric shrinkage of coatings as a function of conversion and the proposed model with equations (11) and (12) shown in the figure, and (d) the internal stress of coatings as a function of the conversion, using beam deflection method and the proposed model
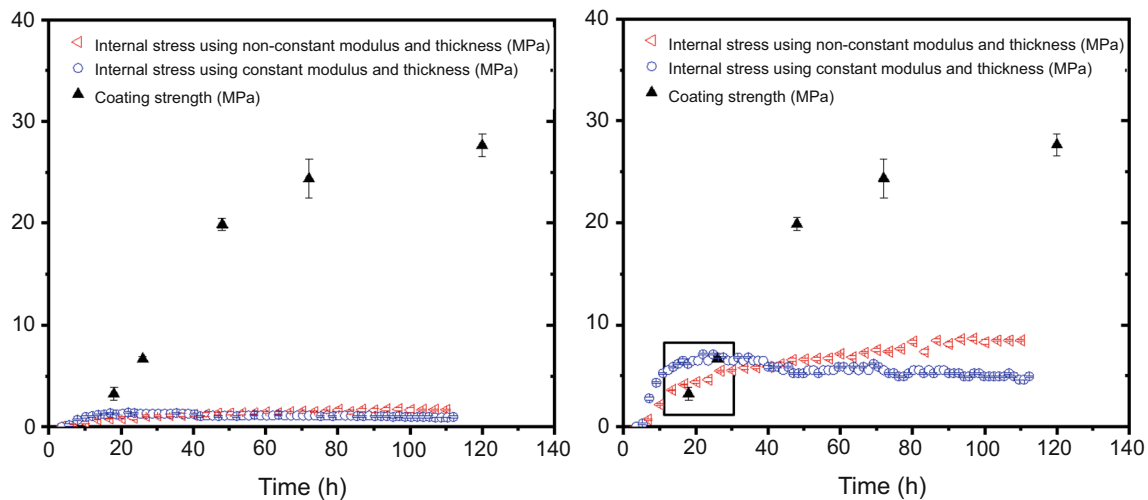
Fig. 8: Comparison of the coating strength and the curing-induced internal stress magnitudes in the epoxy/MXDA coatings on flexible substrates, assuming a stress concentration factor of 1.0 (left) and 5.0 (right). The square in the right-hand figure indicates where the internal stress is larger than or equal to the coating strength and cracking initiation and propagation can take place on rigid substrates

geneities, a crossover of the curing-induced internal stress and coatings strength (marked with a rectangle in the right-hand figure in Fig. 8) may occur, meaning that defects and cracks can initiate and propagate from this curing time and onwards.

In addition, the assumption of a constant coating modulus in the quantification of the internal stress from the deflection method will result in a larger stress during earlier curing times and smaller stress in the final cured coatings, confirming again that constant modulus should not be used with the deflection method.

Conclusions

Using the beam deflection method in combination with an ATR-FTIR spectroscopy, a 3D profilometer, and DMTA experiments, transient properties of coatings during curing, including conversion, modulus, volumetric shrinkage, and internal stress, could be obtained.

Results show that when evaluating the curing-induced internal stress in epoxy/amine coatings with the beam deflection method, the elastic modulus development and thickness change resulting from shrinkage all have a great influence. When using the fully cured coating modulus and the initial coating thickness, while ignoring the coating modulus and thickness change, this provides imprecise estimations of the curing-induced internal stress. Prior to the coating reaching the maximum modulus, the assumption causes overestimation of the internal stress, while later, the assumption can lead to incorrect conclusions regarding the internal stress decrease.

Curing-induced internal stress can be estimated reliably with a rather simple equation based on conversion, coating shear modulus, bulk modulus, and volumetric shrinkage. Furthermore, when a rapid increase in the internal stress is seen, premature coating cracks were prone to initiate after vitrification and prior to the coating reaching the maximum modulus. In order to reduce premature cracks in coatings, formulations or curing conditions that can postpone the point of vitrification and introduce less volumetric shrinkage are preferred.

References

1. Sørensen, PA, Kiil, S, Dam-Johansen, K, Weinell, CE, "Anticorrosive Coatings: A Review." *J. Coat. Technol. Res.*, **6** (2) 135–176 (2009)

2. Møller, VB, Dam-Johansen, K, Frankær, SM, Kiil, S, "Acid-Resistant Organic Coatings for the Chemical Industry: A Review." *J. Coat. Technol. Res.*, **14** (2) 279–306 (2017)

3. Lyon, SB, Bingham, R, Mills, DJ, "Advances in Corrosion Protection by Organic Coatings: What We Know and What We Would Like to Know." *Prog. Org. Coat.*, **102** 2–7 (2017)

4. Knudsen, OØ, Forsgren, A, *Corrosion Control Through Organic Coatings*. Taylor & Francis Group, Boca Raton (2006)

5. Atta, AM, Mohamed, NH, Rostom, M, Al-Lohedan, HA, Abdullah, MMS, "New Hydrophobic Silica Nanoparticles Capped with Petroleum Paraffin Wax Embedded in Epoxy Networks as Multifunctional Steel Epoxy Coatings." *Prog. Org. Coat.*, **128** (October) 99–111 (2019)

6. Wang, K, Varela, FB, Tan, MY, "Probing Dynamic and Localised Corrosion Processes on Buried Steel Under Coating Disbondments of Various Geometries." *Corros. Sci.*, **150** (January) 151–160 (2019)

7. Song, EH, Lee, HI, Chung, MK, Lee, SK, Beak, KK, "Study on the Causes of Premature Cracking of Epoxy Coatings for Ship's Ballast Tanks." *Corros. Sci. Technol.*, **5** (2) 69–76 (2006)

8. Kiil, S, "Quantification of Simultaneous Solvent Evaporation and Chemical Curing in Thermoset Coatings." *J. Coat. Technol. Res.*, **7** (5) 569–586 (2010)

9. Francis, LF, McCormick, AV, Vaessen, DM, Payne, JA, "Development and Measurement of Stress in Polymer Coatings." *J. Mater. Sci.*, **37** 4717–4731 (2002)

10. Nichols, ME, "Anticipating Paint Cracking: The Application of Fracture Mechanics to the Study of Paint Weathering." *J. Coat. Technol.*, **74** (924) 39–46 (2002)

11. Thouless, MD, "Combined Buckling and Cracking of Films." *J. Am. Ceram. Soc.*, **76** (11) 2936–2938 (1993)

12. Thouless, MD, "Some Mechanics for the Adhesion of Thin Films." *Thin Solid Films*, **181** (1–2) 397–406 (1989)

13. Thouless, MD, Hutchinson, JW, Liniger, EG, "Plane Strain, Buckling-Driven Delamination of Thin Films: Model Experiments and Mode-II Fracture." *Acta Metall. Mater.*, **40** (10) 2639–2649 (1992)

14. Chowdhury, M, Sheng, X, Ziebert, F, Yang, ACM, Sepe, A, Steiner, U, Reiter, G, "Intrinsic Stresses in Thin Glassy Polymer Films Revealed by Crack Formation." *Macromolecules*, **49** (23) 9060–9067 (2016)

15. Kandil, FA, Lord, JD, Fry, AT, Grant, PV, "A Review of Residual Stress Measurement Methods—A Guide to Technical Selection." *NPL Rep. MATC (A)*, **4** (January) 1–42 (2001)

16. Withers, PJ, Bhadeshia, HKDH, "Residual Stress Part 1—Measurement Techniques." *Mater. Sci. Technol.*, **17** (4) 355–365 (2001)

17. Shokrieh, MM, Ghanei Mohammadi, AR, "Non-destructive Testing (NDT) Techniques in the Measurement of Residual Stresses in Composite Materials: An Overview." In: *Residual Stresses in Composite Materials*, pp. 58–75. Woodhead Publishing Limited, 2014

18. Yan, X, Ohsawa, T, "Measurement of the Internal Local Stress Distribution of Composite Materials by Means of Laser Imaging Methods." *Composites*, **25** (6) 443–450 (1994)

19. Shiga, T, Narita, T, Tachi, K, Okada, A, Takahashi, A, Kurauchi, T, "Measurement of Internal Stresses in Polymeric Coatings Using Time Resolved Fluorescence." *Polym. Eng. Sci.*, **37** (1) 24–30 (1997)

20. De la Vega, A, Kovacs, JZ, Bauhofer, W, Schulte, K, "Combined Raman and Dielectric Spectroscopy on the Curing Behaviour and Stress Build Up of Carbon Nanotube-Epoxy Composites." *Compos. Sci. Technol.*, **69** (10) 1540–1546 (2009)

21. Abadias, G, Chason, E, Keckes, J, Sebastiani, M, Thompson, GB, Barthel, E, Doll, GL, Murray, CE, Stoessel, CH,

Martinu, L, "Review Article: Stress in Thin Films and Coatings: Current Status, Challenges, and Prospects." *J. Vac. Sci. Technol. A.*, **36** (2) 020801 (2018)

22. Boerman, AE, Perera, DY, "Measurement of Stress in Multicoat Systems." *J. Coat. Technol.*, **70** (881) 69–75 (1998)

23. Croll, SG, "An Overhanging Beam Method for Measuring Internal Stress in Coatings." *J. Oil Colour Chem. Assoc.*, **63** (7) 271–275 (1980)

24. Wen, M, Scriven, LE, McCormick, AV, "Differential Scanning Calorimetry and Cantilever Deflection Studies of Polymerization Kinetics and Stress in Ultraviolet Curing of Multifunctional (Meth)acrylate Coatings." *Macromolecules*, **35** (1) 112–120 (2002)

25. Knudsen, OØ, Bjørgum, A, Frydenberg, T, Johnsen, R, "Development of Internal Stress in Organic Coatings During Curing and Exposure." *NACE - Int. Corros. Conf. Ser.*, (January) 060281–0602810, 2006

26. Abdelkader, AF, White, JR, "Curing Characteristics and Internal Stresses in Epoxy Coatings: Effect of Crosslinking Agent." *J. Mater. Sci.*, **40** (8) 1843–1854 (2005)

27. Abdelkader, AF, White, JR, "Influence of Relative Humidity on the Development of Internal Stresses in Epoxy Resin Based Coatings." *J. Mater. Sci.*, **37** 4769–4773 (2002)

28. Inoue, Y, Kobatake, Y, "Effect of Fillers on Residual Stress in Coatings." *Kollold-Zeitschrift*, **159 H. I** 18–24 (1958)

29. Perera, DY, "Effect of Pigmentation on Organic Coating Characteristics." *Prog. Org. Coat.*, **50** (4) 247–262 (2004)

30. Croll, S, "Effect of Solvent on Residual Strain in Clear Epoxy Coatings." *J. Oil Colour Chem. Assoc.*, **6** (63) 230–236 (1980)

31. O'Brien, DJ, Mather, PT, White, SR, "Viscoelastic Properties of an Epoxy Resin During Cure." *J. Compos. Mater.*, **35** (10) 883–904 (2001)

32. Yi, C, Rostron, P, Vahdati, N, Gunister, E, Alfantazi, A, "Curing Kinetics and Mechanical Properties of Epoxy Based Coatings: The Influence of Added Solvent." *Prog. Org. Coat.*, **124** 165–174 (2018)

33. Rodríguez, MT, Gracenea, JJ, Kudama, AH, Suay, JJ, "The Influence of Pigment Volume Concentration (PVC) on the Properties of an Epoxy Coating: Part I. Thermal and Mechanical Properties." *Prog. Org. Coat.*, **50** (1) 62–67 (2004)

34. Billotte, C, Bernard, FM, Ruiz, E, "Chemical Shrinkage and Thermomechanical Characterization of an Epoxy Resin During Cure by a Novel In Situ Measurement Method." *Eur. Polym. J.*, **49** (11) 3548–3560 (2013)

35. Zobeiry, N, Vaziri, R, Poursartip, A, "Computationally Efficient Pseudo-Viscoelastic Models for Evaluation of Residual Stresses in Thermoset Polymer Composites During Cure." *Compos. A Appl. Sci. Manuf.*, **41** (2) 247–256 (2010)

36. Radue, MS, Varshney, V, Baur, JW, Roy, AK, Odegard, GM, "Molecular Modeling of Cross-Linked Polymers with Complex Cure Pathways: A Case Study of Bismaleimide Resins." *Macromolecules*, **51** (5) 1830–1840 (2018)

37. Simon, SL, Mckenna, GB, Sindt, O, "Modeling the Evolution of the Dynamic Mechanical Properties of a Commercial Epoxy During Cure After Gelation." *J. Appl. Polym. Sci.*, **76** (4) 495–508 (2000)

38. Rabearison, N, Jochum, C, Grandidier, JC, "A FEM Coupling Model for Properties Prediction During the Curing of an Epoxy Matrix." *Comput. Mater. Sci.*, **45** (3) 715–724 (2009)

39. Alig, I, Lellinger, D, Wenzel, M, Holst, M, Xu, J, Böhm, F, Woicke, N, Rodriguez Sánchez, A, "Monitoring and Simulation of Thermoset Curing." *Micromater. Nanomater.*, **11** 132–135 (2009)

40. Alig, I, Oehler, H, Lellinger, D, Tadjbach, S, "Monitoring of Film Formation, Curing and Ageing of Coatings by an Ultrasonic Reflection Method." *Prog. Org. Coat.*, **58** (2–3) 200–208 (2007)

41. Holst, M, Schänzlin, K, Wenzel, M, Xu, J, Lellinger, D, Alig, I, "Time-Resolved Method for the Measurement of Volume Changes During Polymerization." *J. Polym. Sci. B Polym. Phys.*, **43** (17) 2314–2325 (2005)

42. Alig, I, Steeman, PAM, Lellinger, D, Dias, AA, Wienke, D, "Polymerization and Network Formation of UV-Curable Materials Monitored by Hyphenated Real-Time Ultrasound Reflectometry and Near-Infrared Spectroscopy (RT-US/NIRS)." *Prog. Org. Coat.*, **55** (2) 88–96 (2006)

43. Nawab, Y, Shahid, S, Boyard, N, Jacquemin, F, "Chemical Shrinkage Characterization Techniques for Thermoset Resins and Associated Composites." *J. Mater. Sci.*, **48** (16) 5387–5409 (2013)

44. Shah, DU, Schubel, PJ, "Evaluation of Cure Shrinkage Measurement Techniques for Thermosetting Resins." *Polym. Test.*, **29** (6) 629–639 (2010)

45. Shenogina, NB, Tsige, M, Mukhopadhyay, SM, Patnaik, SS, "Molecular Modeling of Thermosetting Polymers: Effects of Degree of Curing and Chain Length on Thermo-Mechanical Properties." *18th ICCM Int. Conf. Compos. Mater.*, Jeju Island, Korea, August 2011

46. Wise, CW, Cook, WD, Goodwin, AA, "Chemico-Diffusion Kinetics of Model Epoxy-Amine Resins." *Polymer*, **38** (13) 3251–3261 (1997)

47. Horie, K, Mita, I, Kambe, H, "Calorimetric Investigation of Polymerization Reactions. IV. Curing Reaction of Polyester Fumarate with Styrene." *J. Polym. Sci. A-1 Polym. Chem.*, **8** (10) 2839–2852 (2003)

48. Chern, C-S, Poehlein, GW, "A Kinetic Model for Curing Reactions of Epoxides with Amines." *Polym. Eng. Sci.*, **27** (11) 788–795 (1987)

49. Achilias, DS, Karabela, MM, Varkopoulou, EA, Sideridou, ID, "Cure Kinetics Study of Two Epoxy Systems with Fourier Transform Infrared Spectroscopy (FTIR) and Differential Scanning Calorimetry (DSC)." *J. Macromol. Sci. A Pure Appl. Chem.*, **49** (8) 630–638 (2012)

50. Jenninger, W, Schawe, JEK, Alig, I, "Calorimetric Studies of Isothermal Curing of Phase Separating Epoxy Networks." *Polymer*, **41** (4) 1577–1588 (2000)

51. Fournier, J, Williams, G, Duch, C, Aldridge, GA, "Changes in Molecular Dynamics During Bulk Polymerization of an Epoxide-Amine System as Studied by Dielectric Relaxation Spectroscopy." *Macromolecules*, **29** (22) 7097–7107 (1996)

52. Xu, J, Holst, M, Rüllmann, M, Wenzel, M, Alig, I, "Reaction-Induced Phase Separation in a Polysulfone-Modified Epoxy-Anhydride Thermoset." *J. Macromol. Sci. B Phys.*, **46B** (1) 155–181 (2007)

53. Li, C, Potter, K, Wisnom, MR, Stringer, G, "In-Situ Measurement of Chemical Shrinkage of MY750 Epoxy Resin by a Novel Gravimetric Method." *Compos. Sci. Technol.*, **64** (1) 55–64 (2004)

54. Perera, DY, "Stress Phenomena in Organic Coatings." In: *Paint and Coating Testing Manual: 15th Edition* (MNL17), ASTM, pp. 655–672, 2012

55. Jochum, Ch, Arrigoni, M, Boustie, M, Grandidier, JC, "Estimation of the Residual Stress State Generated During the Curing of A Thick Epoxy Matrix by Pulsed Laser." *ECCM16-16TH European Conference on Composite Materials*, Seville, Spain, June 2014

56. Prasatya, P, McKenna, GB, Simon, SL, "A Viscoelastic Model for Predicting Isotropic Residual Stresses in Ther-

mosetting Materials: Effects of Processing Parameters.'' *J. Compos. Mater.*, **35** (10) 826–848 (2001)

57. Rabearison, N, Jochum, C, Grandidier, JC, ''FEM Simulation of a Thermosetting Epoxy Matrix: Application to Internal Stresses.'' *16th ICCM Int. Conf. Compos. Mater.*, Kyoto, Japan, July 2007

58. Kiil, S, ''Mathematical Modelling of Simultaneous Solvent Evaporation and Chemical Curing in Thermoset Coatings: A Parameter Study.'' *Prog. Org. Coat.*, **70** (4) 192–198 (2011)

59. Yu, H, Mhaisalkar, SG, Wong, EH, ''Observations of Gelation and Vitrification of a Thermosetting Resin During the Evolution of Polymerization Shrinkage.'' *Macromol. Rapid Commun.*, **26** (18) 1483–1487 (2005)

60. Kroll, DM, Croll, SG, ''Heterogeneity in Polymer Networks Formed by a Single Copolymerization Reaction: II. Postgelation Structure and Pendants.'' *Polymer*, **116** 113–123 (2017)